

1 **Low Temperatures Enhance Organic Nitrate Formation:**
2 **Evidence from Observations in the 2012 Uintah Basin**
3 **Winter Ozone Study**

4
5 **L. Lee¹, P. J. Wooldridge¹, J. B. Gilman², C. Warneke², J. de Gouw² and R. C.**
6 **Cohen^{1,3}**

7 [1]{Department of Chemistry, University of California, Berkeley, CA, USA}

8 [2]{Chemical Science Division, Earth System Research Laboratory, National Oceanic &
9 Atmospheric Administration, Boulder, CO, USA}

10 [3]{Department of Earth and Planetary Sciences, University of California, Berkeley, CA,
11 USA}

12
13 Correspondence to: R. C. Cohen (rccohen@berkeley.edu)

14
15 **Abstract**

16 Nitrogen dioxide (NO₂) and total alkyl nitrates (ΣANs) were measured using thermal
17 dissociation laser induced fluorescence during the 2012 Uintah Basin Winter Ozone Study
18 (UBWOS) in Utah, USA. The observed NO₂ concentration was highest before sunrise and
19 lowest in the late afternoon, suggestive of a persistent local source of NO₂ coupled with
20 turbulent mixing out of the boundary layer. In contrast, ΣANs co-varied with solar radiation
21 with a noontime maximum, indicating that local photochemical production combined with
22 rapid mixing and/or deposition was the dominant factor in determining the ΣAN
23 concentrations. We calculate that ΣANs were a large fraction (~ 60%) of the HO_x free radical
24 chain termination and show that the temperature dependence of the alkyl nitrate yields
25 enhances the role of ΣANs in local chemistry during winter by comparison to what would
26 occur at the warmer temperatures of summer.

1 **1 Introduction**

2 The Uintah Basin in Utah is a region of concentrated fossil fuel extraction operations using
3 hydraulic fracturing to extract natural gas and oil from shale formations. The basin has
4 experienced high wintertime ozone as has the nearby Upper Green River Basin in Wyoming
5 (Schnell et al., 2009). The observed ~200 ppb peak ozone in the basin during the winter of
6 2011 was associated with elevated concentrations of volatile organic compounds (VOCs)
7 coincident with a shallow boundary layer stabilized by snow cover, which doubled as a solar
8 reflector leading to more rapid photochemistry.

9
10 Organic nitrates (RONO_2) are products of atmospheric VOC oxidation in the presence of NO_x
11 ($\text{NO} + \text{NO}_2$). During daytime, their formation involves the association reaction of alkyl
12 peroxy radicals with NO. This reaction terminates ozone formation and suppresses OH
13 recycling. The importance of RONO_2 formation as a NO_x sink and chain terminator of ozone
14 production depends on the mixture of VOCs present as a result of variations in OH reactivity
15 and organic nitrate yield, α , among different organic molecules (Perring et al., 2013; Farmer
16 et al., 2011). Laboratory studies have shown that the nitrate yield follows standard
17 expectations for 3-body reactions: α increases with carbon number of the organic peroxy
18 radical and atmospheric pressure, but decreases with temperature (Atkinson et al., 1983;
19 Carter and Atkinson, 1989). Field observations have found RONO_2 compounds to account for
20 25% or more of total reactive nitrogen (NO_y , defined as $\text{NO}_x +$ higher nitrogen oxides).
21 However, none of these prior field experiments (Farmer et al., 2011; Rosen et al., 2004;
22 Perring et al., 2010; Perring et al., 2009) covered a temperature range wide enough to
23 examine the role of the temperature dependence of α on nitrate formation rates, O_3 , or OH
24 concentrations.

25
26 In this paper we present observations of organic nitrates obtained during the UBWOS 2012
27 experiment (15 January–29 February 2012). We further describe the role of organic nitrates in
28 wintertime ozone production and the associated temperature effect by comparing the α values
29 either constrained by observed ΣANs concentration or derived from temperature-dependent
30 yields from VOC composition data. The findings show organic nitrate formation to be one of
31 the primary radical sinks at this site and confirm that the temperature-dependent kinetics are

1 important. However, temperature dependence of organic nitrate yields are not presented in
2 any of the standard photochemical mechanisms used in chemical transport models.
3 Accounting for the temperature dependent yields at 0°C (the typical daytime temperature
4 during this field campaign) results in a 30% faster organic nitrate formation rate than what
5 would occur at room temperature (300K). As a result, we estimate a suppression in OH
6 concentrations by 15% and ozone formation by 20% relative to the calculations that do not
7 include the temperature dependence of the RONO₂ yields.

8 9 **2 Instrumentation**

10 The 2012 Uintah Basin Winter Ozone Study occurred from January 15th to the end of
11 February at Horse Pool, Utah, a site approximately 30 miles south of the city of Vernal, Utah.
12 This site was located amid intensive oil and gas extraction operations near the center of
13 Uintah Basin, with dense gas production wells to the south and oil production wells to the
14 south-west (refer to Fig. 1 of Edwards et al., 2013). A 19 meter high tower was on-site for
15 setting up measurements at various heights.

16
17 Thermal Dissociation-Laser Induced Fluorescence (TD-LIF) was used to measure NO₂, total
18 peroxy nitrates (Σ PNs = Σ ROONO₂) and total alkyl nitrates (Σ ANs = Σ RONO₂) using
19 methods described previously. (Day et al., 2002; Thornton et al., 2000) Briefly, laser induced
20 fluorescence was used for detection of gas phase NO₂ using a pulsed tunable fiber laser (~80
21 mW, NovaWave) at 530 nm for excitation with detection of photons at wavelengths longer
22 than 700 nm using a red-sensitive PMT (Hamamatsu H7421) preceded by a dielectric long-
23 pass filter. Quartz tubes with external heating elements were maintained at 180°C for
24 conversion of Σ PNs and 380°C for Σ ANs to NO₂ under a residence time of ~0.17 seconds.
25 The air sample passing through the heated regions were under near ambient atmospheric
26 pressure before entering a restrictive orifice into low pressure transfer line to the LIF cell.
27 Simultaneous measurements of NO₂, Σ PNs and Σ ANs were achieved by operating 3 LIF cells,
28 each measuring the cumulative concentration of NO₂-yielding compounds.

29
30 Laboratory experiments carried out after the deployment indicate that the Σ ANs channel had
31 been set to a temperature that was higher than necessary to fully dissociate alkyl nitrates. The

1 O₃ pyrolysis and subsequent O atom-initiated chemistry that is usually a very minor negative
2 interferences (Day et al., 2002) resulted in a large enough effect to require a correction term
3 for this dataset. The correction is an empirical relationship developed in the laboratory by
4 directly observing the loss of the 380°C signal as a function of both O₃ and NO₂
5 concentrations in the presence of an organic nitrate surrogate (2-ethylhexyl nitrate, Sigma
6 Aldrich). Details of this correction are included in the Appendix A. The factors applied during
7 the daytime hours that are the focus of this study were typically 6–17% of the total 380°C
8 signal, of which ΣANs account for approximately 25%. This amounts to a correction of
9 24–68% of the final ΣANs concentration. Larger corrections were required at night due to
10 higher NO₂ concentration. There are also additional contributions from inorganic species,
11 including N₂O₅ (which decomposes to NO₂ and NO₃ at ~90°C) in the 180°C channel and
12 ClNO₂ (which decomposes to a chlorine atom and NO₂ (Thaler et al., 2011)) in the 380°C
13 channel. However, accounting for the inorganic signal was straightforward since direct
14 measurements of both species were available at the site. (Wagner et al., 2011; Roberts et al.,
15 2009) Overall, the ClNO₂ contribution to the difference signal between 380°C and 180°C was
16 only significant during the night and early morning since, for example, the noontime
17 photolysis lifetime of ClNO₂ is only 1 hour. We note that N₂O₅, present only during
18 nighttime, did not affect daytime ΣPNs measurements.

19

20 In subsequent analyses, ΣPNs is calculated as the difference in concentrations of the ambient
21 and 180°C channel minus the N₂O₅ contribution, while ΣANs is the concentration difference
22 between the 180°C channel and the O₃-corrected 380°C channel minus the ClNO₂
23 contribution.

24

25 The TD-LIF instrument was calibrated hourly with a 5 ppm NO₂ gas standard diluted with
26 zero air to generate 5 different concentration levels at the inlet manifold. In addition, the
27 instrument zero (baseline) was monitored every half-hour by overflowing the inlet with NO_x-
28 free zero air. The NO₂ concentration measured by LIF and nearby chemiluminescence
29 instrument were within 7% of each other on average, giving a linear slope (LIF vs.
30 chemiluminescence) of 0.94, an intercept of 0.02 ppb, and an R² value of 0.97.

31

1 The inlet was mounted on the southern face of the tower, 16 m above the ground. Other
2 measurements made from similar heights include NO and NO_y (Kliner et al., 1997), speciated
3 VOCs (Goldan et al., 2004), O₃ and photolysis rates for O₃ (O¹D), NO₂ and NO₃. These
4 measurements are described elsewhere (see description and Table S1 in Edwards et al., 2013).
5 Temperature, pressure, relative humidity, wind direction and windspeed were measured from
6 the top of the tower. 3D wind data were measured using the High Resolution Doppler Lidar
7 (Grund et al., 2001) nearby.

8

9 **3 Results**

10 **3.1 Observations**

11 Figure 1 shows the time series (as hourly average) of NO₂, ΣANs, O₃ and windspeed through
12 the observational period. The time-of-day median values of NO₂, ΣANs and O₃ are plotted in
13 Figure 2. During periods with windspeed lower than 5 m/s, the chemical species, such as large
14 volatile organic compounds (VOCs) and NO_x, accumulate, leading to an increase in
15 concentrations until high wind episodes occur that flush the basin with clean air. The onset of
16 high wind episodes were therefore coincident with a rapid decrease in VOCs and NO_x
17 concentrations. During the UBWOS campaign in the year before (2011), up to 200 ppb ozone
18 was observed at the end of accumulation periods with snow cover on the ground. However,
19 during similar period in the 2012 campaign, there was little snow and the ozone concentration
20 did not exceed 51 ppb.

21

22 **3.1.1 NO₂**

23 NO₂ showed a clear diurnal variation (Figure 2). Concentrations were highest in the early
24 morning when vehicle traffic as well as oil well machinery emissions became coincident with
25 a stable nocturnal boundary layer. Turbulent mixing in the afternoon diluted the
26 concentration, giving a minimum at 4 pm local time. The multi-day effect of high/low wind
27 episodes on NO₂ concentration is visible for which high windspeed always corresponds to
28 low NO₂ levels (Figure 1).

29

1 **3.1.2 Σ ANs**

2 The daily variation in Σ ANs concentration is less pronounced than for NO_2 but follows a
3 similar multi-day trend controlled by meteorology. As shown in Figure 2, the total RONO_2
4 concentration increases in the morning to a noon time peak of 1.5 ppb. The contributions from
5 C_1 - C_3 alkyl nitrates measured by GC-MS are small and nearly constant at ~ 50 ppt and did not
6 contribute to the diurnal profile observed.

8 **3.1.3 O_3**

9 The observed O_3 concentration ranged from 4 to 50 ppb and was negatively correlated with
10 NO_2 . The diurnal profile has a maximum concentration in the late afternoon, corresponding to
11 a delay of roughly 4 hours from the peak of organic nitrates. The increase in O_3 concentration
12 is most rapid (~ 2.4 ppb hour^{-1}) at noon.

14 **3.1.4 VOCs**

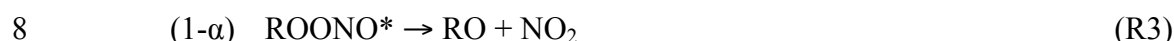
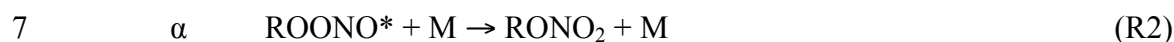
15 The VOC composition is influenced heavily by the fossil fuel extraction operations. Alkane
16 oxidation dominates the chemistry in the basin (Table 1), accounting for 67% of total
17 measured VOC reactivity (7.5 s^{-1}) at noon. The diurnal profile of VOCs follows NO_2 ,
18 reaching a minimum in the late afternoon (see Figure 3a in Edwards et al., 2012).

20 **3.2 The average branching ratio for nitrate formation**

21 The average noontime temperature during the UBWOS experiment was 0°C . These cold
22 temperatures provide a unique opportunity to examine the role of temperature on the
23 formation of organic nitrates and the associated radical chain termination compared with other
24 field campaigns taking places in summer.

25
26 Organic nitrate compounds are formed via OH-initiated oxidation. For the specific mixture of
27 VOCs observed, the dominant reaction starts with hydrogen abstraction from alkanes by OH.
28 The resulting alkyl radical rapidly reacts with O_2 to give alkyl peroxy radical RO_2 , which

1 subsequently reacts with NO to form an energy-rich adduct of the structure ROONO*
 2 (Reaction R1). Under typical atmospheric conditions, a fraction (Reaction R2) of ROONO* is
 3 collisionally stabilized to form the nitrooxy group, RONO₂, while the unstabilized portion
 4 (Reaction R3) dissociates to yield an alkoxy radical and NO₂. The fate of the alkoxy radical
 5 varies depending on the carbon backbone but, in general, returns a HO₂ radical.



9 Given a rate of VOC reaction with OH, the key factor regulating RONO₂ production is the
 10 nitrate branching ratio, α , defined as the overall fraction of the RO₂ + NO reaction that gives
 11 an organic nitrate product rather than an alkoxy radical and NO₂ product. The association
 12 reaction to form RONO₂ is compound-specific and temperature- and pressure-dependent
 13 (Atkinson et al., 1983). In the subsequent sections, we present 2 independent methods for
 14 estimating ensemble-averaged α values (or $\langle\alpha\rangle$) for the specific environment of UBWOS
 15 campaign, and demonstrate they agree to within the uncertainty of our observations. The first
 16 method (section 3.2.1) is based on parameterizations derived from laboratory experiments and
 17 the observed VOC composition data, while the second method (section 3.2.2) uses the
 18 observed Σ ANs concentration, photolysis and VOC reactivity.

19

20 **3.2.1 VOC-ensemble method**

21 The averaged α , $\langle\alpha\rangle$, is defined in equation below as the summation of compound-specific α
 22 values weighted by their relative importance in atmospheric oxidation calculated as the
 23 product of OH reaction rate constant and compound concentration (namely, the OH
 24 reactivity).

$$25 \quad \langle\alpha\rangle = \frac{\sum_i k_i[x_i]\alpha_i}{\sum_j k_j[x_j]} \quad (1)$$

26 Here α_i denotes the compound-specific nitrate branching ratio, k_i (k_j) the OH reaction rate
 27 constant and $[x_i]$ ($[x_j]$) the concentration of species i (j). The VOC OH reactivity, $k_i[x_i]$ ($k_j[x_j]$),
 28 in the Uintah basin was dominated by alkanes (see Table 1). We point out here that the net
 29 effect of temperature on the OH reaction rate constants was generally small, typically a 5%

1 reduction in total OH reactivity compared with 298K values (Atkinson, 1994) and the
2 dominant temperature dependence of organic nitrate production is due to the nitrate branching
3 ratio as detailed below.

4
5 For α_i specific to alkanes, we use temperature- and pressure-dependent, compound-specific α_i
6 values (Carter and Atkinson, 1989) and include contributions of secondary organic nitrate
7 formation after alkoxy radical isomerization reactions which can be increasingly important for
8 alkanes larger than butane. This increases the individual organic nitrate yield by up to 30%,
9 generally proportional to the size of the molecule. The compound-specific α values are
10 summarized in Table 2.

11
12 The α_i value for aldehydes were treated as having the same nitrate yield as the RO_2 having
13 one less carbon, since the major reaction with OH involves aldehydic hydrogen abstraction
14 and decomposition following reaction with NO to give a CO_2 and a C_{n-1} alkyl radical. α for
15 ketones were estimated using the same method as detailed for alkanes. Methanol and ethanol
16 are presumed to have zero nitrate yield, since their reactions with O_2 after hydrogen
17 abstraction to form carbonyls and HO_2 are dominant. Finally, the nitrate yields for aromatics
18 were set to 1% in this analysis, following the yield of benzyl nitrate from toluene oxidation
19 (Gery et al., 1985; Atkinson and Aschmann, 1989; Atkinson, 1994). It is noted that even by
20 assuming an upper-limit nitrate yield of 0.35, the contribution from aromatic compounds to
21 alkyl nitrate production is minor (14%) relative to the production from alkanes.

22
23 The average nitrate formation yield, $\langle\alpha\rangle$, as calculated above including all VOC and CO
24 measurements throughout the campaign period, is plotted in Figure 3 as instantaneous values
25 (gold) and as a daytime (8am–6pm) average (red filled symbol). The organic nitrate yield
26 ranged from 3% to 15% with low values corresponding to periods of high winds (e.g. 3
27 February). Variation in VOC concentration and composition is the dominant factor
28 controlling the day to day variation as well as the variation over each day. Daytime averaged
29 values of $\langle\alpha\rangle$ calculated at a temperature of 300K are shown in blue. Even at 300K the $\langle\alpha\rangle$ is
30 significant, often around 10%.

31
8

1 3.2.2 Oxidation-production method

2 Our second approach to estimating α is based primarily on the Σ AN measurements. In this
3 case, $\langle\alpha\rangle$ can be expressed as the ratio of the Σ AN production rate over the total VOC
4 consumption rate (Eq. 2a).

$$5 \quad \langle\alpha\rangle = \frac{p(\Sigma ANs)}{[OH] \cdot \sum_i k_i [x_i]} \quad (2a)$$

$$6 \quad p(\Sigma ANs) = \frac{d(\Sigma ANs)}{dt} + k_{mix} \cdot \Sigma ANs \quad (2b)$$

$$7 \quad [OH] = f(\sum_i k_i [x_i], J, \langle\alpha'\rangle) \quad (2c)$$

8 The individual terms in Eq. (2a) can be derived from observations, as shown in Eq. (2b) and
9 (2c). The total production rate of Σ ANs ($p(\Sigma ANs)$) is expressed, according to mass balance, as
10 the sum of the rate of change of the observed Σ AN concentration and an overall loss term in
11 Eq. (2b). Chemical losses of Σ ANs are found to be negligible compared with turbulent mixing
12 out of the boundary layer. To estimate this effective loss rate constant " k_{mix} ", we employ a
13 tracer method by solving Eq. (2b) using n-propyl nitrate concentrations measured by GC-MS.
14 We chose n-propyl nitrate because its expected loss is also dominated by mixing due to the
15 long chemical lifetime, and its production rate can be calculated independently from
16 measured VOC precursors. Note here that the OH concentration is needed to calculate the
17 production rate of n-propyl nitrate, as well as the VOC consumption rate in the denominator
18 of Eq. (2a). The OH concentration is a function of VOC reactivity and photolysis rates (J
19 values) as well as the α value for the radical recycling efficiency. Due to the dependence of
20 the OH concentration on the nitrate yield, it is not possible to represent α in a closed
21 functional form using all other variables. Therefore, the set of equations must be solved
22 iteratively until a self-consistent α and OH concentration are obtained ($\langle\alpha\rangle = \langle\alpha'\rangle$).

23

24 The calculations proceed as follows by calculating the following: (1) OH concentration and
25 VOC consumption rate, (2) mixing rate estimates, (3) Σ ANs formation rate and $\langle\alpha\rangle$.

26

27 (1) *OH concentration and VOC consumption rate:*

28 We used photolysis rates of O_3 , NO_2 , NO_3 , HONO, ClNO₂, acetaldehyde, acetone,
29 formaldehyde and HNO₃ to calculate OH and HO₂ production rates. Photolysis rates for O_3 ,

1 NO₂ and NO₃ are measured directly with filter radiometers. For other species they are
2 estimated using linear combination of photolysis rates of O₃ and NO₂. OH formation from
3 alkene ozonolysis reactions was negligible. The medium total radical production of 2.5
4 ppb/day is similar to the value reported by Edwards et al., 2013. Data for NO, NO₂ and VOCs
5 coupled with literature values of OH reaction rate constants corrected for campaign measured
6 temperature and pressure dependence (Atkinson et al., 2004, 2006) were then used for OH
7 and HO₂ calculations including radical recycling. The resulting VOC consumption rate is
8 shown in Figure 4. Note the VOC consumption rate profile conforms more to the shape of the
9 radical source strength (OH and HO₂ formation rate derived from photolysis, same shape as
10 solar irradiation) than to the OH concentration, consistent with the notion that VOCs are the
11 major reaction partner with OH.

12

13 (2) *Mixing rate estimation:*

14 We estimate the dilution loss (k_{mix}) for Σ ANs concentration by substituting [Σ ANs] with n-
15 propyl nitrate concentration in Eq. 2b. The time derivative of n-propyl nitrate concentration
16 was calculated using a finite difference method, followed by application of a 2-hour running
17 mean to smooth hourly data. Kinetic studies dictate that ~24% of the OH reaction with
18 propane at 273K yielded a primary alkyl radical, (Droege and Tully, 1986) which promptly
19 reacted with O₂ to form the corresponding peroxy radical. Larger alkane molecules can also
20 yield n-propyl alkyl radical as a result of alkoxy radical decomposition from the appropriate
21 structure, and we accounted for all such minor formation channels up to undecane to give a
22 total additional contribution of 14% from sources other than propane. The total formation rate
23 of n-propyl nitrate is presented in Figure 5 as the red trace spanned by the 25 and 75
24 percentiles in the shaded area. Plotted in blue is the median value of time derivative of n-
25 propyl nitrate concentration showing a diurnal pattern for which peak concentration was
26 reached at noon time when the time derivative crosses the zero line. The initial concentration
27 increase roughly coincides with the start of photochemical reaction, as is also marked by the
28 onset of n-propyl nitrate formation rate. The negative portion of the blue trace in the afternoon
29 then corresponds to faster dilution due both to turbulence and to the elevated concentration.
30 These values are sufficient to solve for the time-varying dilution rate constant, k_{mix} , shown in
31 Figure 5 as green line with dashed traces bounding the interquartile range. Note the slight
32 delay (~1 hour) in the daily maximum of the dilution rate constant when compared with the

1 peak of n-propyl nitrate formation rate. As vertical turbulence was promoted by surface
2 heating, this delay is a reasonable consequence of the expected lag in the mixing rate. The
3 median daily maximum mixing rate shows a time constant of 6 hours, much more rapid than
4 other loss processes such as the OH oxidative lifetime of n-propyl nitrate of over 150 hours
5 under the OH concentration of $2 \times 10^6 \text{ cm}^{-3}$ (Figure 4) and a photolysis lifetime of over 200
6 hours, (Luke et al., 1989) consistent with our initial assumption that chemical losses are small.

7

8 (3) Σ ANs formation rate and $\langle \alpha \rangle$:

9 Using the k_{mix} calculated above, the Σ AN formation rate was estimated using Eq. (2b). We
10 then inserted this Σ AN formation rate and VOC consumption rate back into Eq. (2a) to obtain
11 the implied $\langle \alpha \rangle$ value based on the field observations and also the initial guess of $\langle \alpha' \rangle$. For
12 time periods when $\langle \alpha \rangle$ mismatches $\langle \alpha' \rangle$, $\langle \alpha' \rangle$ is adjusted toward $\langle \alpha \rangle$ accordingly and the
13 calculation repeated to achieve consistency. To reduce the number of points needed for
14 calculation, we only estimated one self-consistent $\langle \alpha \rangle$ value for each day by averaging from
15 8am to 6pm, the same as the averaging window used for our first method.

16

17 Direct comparison of the estimate from Sect. 3.2.2 with the one derived from just the VOC
18 composition (Sect. 3.2.1) is shown in Figure 6. There were 27 days to compare and the two
19 methods are nearly identical, yielding a slope of 1.06 and $R^2 = 0.61$. The similarity in results
20 of the two methods lends support to the estimates of α and confirms the importance of a
21 significant temperature dependence to the value of α affecting the UBWOS chemistry.

22

23 **4 Discussion**

24 The relatively high value observed for the average nitrate yield, $\langle \alpha \rangle$, of ~15%, is a direct
25 consequence of low temperatures and the presence of heavy alkanes, a special condition
26 created by natural gas and oil extraction operations in the basin. In the following sections, we
27 discuss how this elevated nitrate yield affects the fate of NO_x emitted into the basin and the
28 rate of local O_3 production.

29

1 **4.1 Fate of NO_x**

2 Organic nitrate formation was a significant chemical loss for NO_x in the Uintah Basin. We
3 calculated that alkyl nitrate formation is 50% faster than HNO₃ formation during the low wind
4 periods, of 0.23 ppb hour⁻¹ vs. 0.16 ppb hour⁻¹ using the estimated noontime OH
5 concentration. Together, this amounts to a NO_x chemical lifetime of 17 hours, with relative
6 branching of 59% to alkyl nitrate formation and 41% to HNO₃ formation. PAN and other
7 peroxyacyl nitrate compounds were not observed to have high production rates based on
8 measured ΣPNs and PAN concentration and direct calculation of their formation rate from
9 VOC composition including aldehydes. We estimate a lower and upper limit in noontime
10 median net production of 0.01 to 0.06 ppb PAN hour⁻¹, using bottom-up (VOC speciation)
11 and top-down (observed PAN concentration and dilution rate assuming zero background PAN
12 concentration) methods, respectively. This corresponds to PAN representing a maximum of
13 ~18% of the NO_x sink. Alkyl nitrate formation is therefore the single most important chemical
14 loss pathway for NO_x as well as the most important terminator for OH chain propagation.
15 Note that, although ΣAN formation is the largest chemical sink, mixing out of the basin is the
16 dominant overall loss for NO_x emitted. We estimate 68% of NO_x loss is to transport out of the
17 basin.

18

19 **4.2 O₃ formation**

20 O₃ formation is closely related to the formation of organic nitrates, since the reaction channels
21 lead from a branching point in a common pathway. Similar to our treatment of VOC-specific
22 α values, we calculated, for each measured VOC molecule, the average number of O₃
23 molecules generated in a single event of OH initiated oxidation, denoted as γ in Table 2. Note
24 that our definition and estimate for γ includes the contribution from multi-generation alkyl
25 nitrate formation, making it slightly different from previous calculations (Rosen et al., 2004;
26 Perring et al., 2013; Farmer et al., 2011) (see Appendix C). The O₃ production rate is then a
27 product of the ensemble-averaged γ and the VOC consumption rate calculated above, as
28 plotted in Figure 7. The difference between the O₃ production rate and the rate of change in
29 O₃ concentration signifies the contribution of mixing into the background air. When
30 compared with the production characteristics of n-propyl nitrate in Figure 4, it is apparent that
31 dilution loss is much more important for the case of n-propyl nitrate (>80% of the formation

1 rate) than for O₃ (~30% of formation rate). Using the k_{mix} derived from n-propyl nitrate
2 formation, the local O₃ budget of the whole campaign period can be closed with a background
3 O₃ concentration in the range of 20–35 ppb, consistent with observations during high wind
4 periods. This also reinforces the notion that our estimate for turbulent mixing is
5 representative. To reproduce the short-term variations in O₃ production over a 72-hour period
6 with a fixed background O₃ level of 30 ppb, we estimate the expected change in O_x (O₃ +
7 NO₂) concentration using the mass balance equation (Eq. 2b) to find reasonable agreement
8 with the observations (Figure 8).

9

10 Regarding the relative production of O₃ to ΣANs, the average $pO_3/p\Sigma ANs$ calculated as γ/α
11 for UBWOS is 15. For comparison, a value of 6.2–7.5 was reported for the Deep Water
12 Horizon (DWH) plume study (Neuman et al., 2012). While both plumes were dominated by
13 alkanes, the VOC suite for the DWH study was further enriched in heavier organics. This is
14 consistent with the understanding that alkyl nitrate yield increases with the carbon number of
15 the precursor alkane. By comparison, a typical industrial city plume (Rosen et al., 2004)
16 measured around Houston during Texas Air Quality Study 2000 has a value of 29–41, a direct
17 result from low α value (6.5%–4.7%) caused by high temperature (~ 40°C) and relatively low
18 contribution from large alkanes.

19

20 **4.3 Temperature**

21 Currently, none of the chemical mechanisms commonly employed in the chemical transport
22 models for regional O₃ predictions have incorporated the temperature dependence of alkyl
23 nitrate yields. Since alkyl nitrate formation is a radical termination reaction, reduction in
24 temperature decreases the OH recycling probability and shortens the OH radical chain length.
25 For the 2012 UBWOS campaign the effect is to reduce the radical propagation chain length
26 from a noontime median of 3.2 (300K) to 2.6 (273K). Since the chain length is directly
27 proportional to the O₃ production rate, this corresponds to a 20% decrease in the O₃ formation
28 rate. Table 3 shows the estimated maximum O_x concentration in a multi-day low wind
29 accumulation event in the Uintah Basin based on the observed alkyl nitrate yield. We
30 compare a calculation at 300K to one at 273K. Note that for a snowless winter condition, such

1 as encountered in UBWOS 2012, the prediction matches well with the observed maximum
2 hourly O_x concentration of 51 ppb in the afternoon of 2/18/2012. While estimating the α value
3 at 300K always yields a higher predicted O₃ concentration, the over prediction is greatest for
4 the simulated snow condition (right most column) when persistent snow cover increases the
5 photolysis rate and stabilizes the boundary layer impeding mixing.

6

7 **5 Conclusion**

8 We presented an analysis of field observations obtained in the Uintah Basin during winter
9 2012 in Utah, USA. We find that the field data can be used to derive the temperature
10 dependence of the ensemble-averaged nitrate yield, <α>, and that this value is consistent with
11 a parameterization derived from laboratory experiments. Including the proper temperature
12 dependence based on the dominating VOC species should be considered for models aimed at
13 estimating local O₃ concentrations in order to avoid substantial errors (+15% at 0°C from
14 27°C values).

15

16 **Appendix A: O₃ pyrolysis correction for ΣANs (380°C) channel**

17 The cause of this interference was O₃ pyrolysis to yield O atom in the TD oven at elevated
18 temperature. In the absence of organic molecules, the O atom can serve as a promoter for NO
19 and NO₂ interconversion reaction, as illustrated in Reactions (R4)–(R7).



24 NO and NO₂ are interconverted at a cost of one O atom whose steady state concentration is
25 generally controlled by the forward and reverse reactions (R4 and R5). If sufficient time is
26 given, NO and NO₂ will ultimately reach an equilibrium ratio which can be calculated from
27 the reaction rate k_{R5} and k_{R6} (of Reactions R5 and R6, respectively) with pressure dependence.
28 From the O₃ pyrolysis rate and the gas residence time of 0.17 second in our TD oven region,
29 only ΣANs channel at 380°C should generate sufficient O atom to significantly alter the NO₂
30 concentration. To confirm this effect, we performed a series of lab experiments under NO_x

1 and O₃ concentrations covering the range observed during the UBWOS campaign in the
2 presence of ~2 ppb of 2-ethylhexyl nitrate, a simple alkyl nitrate standard available from
3 Sigma Aldrich as a surrogate for the collection of ΣANs in Utah. Figure A1 demonstrates the
4 result from a temperature scan experiment when the inlet oven temperature of cell 1 was
5 scanned upward from 180°C to 380°C, the operating temperature of ΣANs channel in the
6 field. The red trace represents the NO₂ signal from cell 1, while the black trace is the NO₂
7 signal from cell 3 whose inlet was unheated. Since there was no peroxy nitrate in the system,
8 at 180°C cell 3 only detect the same amount of NO₂ as the ambient temperature cell 1.
9 However, starting from ~200°C alkyl nitrate started to thermal dissociate, giving extra NO₂
10 signal as the red trace increased relative to the black trace. The proper setting for ΣANs
11 observations would be in the 250°C to 280°C range in this instance. At temperature beyond
12 280°C effects due to O₃ pyrolysis started to reduce the excess NO₂ signal, presumably by the
13 interconversion reaction mentioned above and we see the red trace eventually dropped below
14 the black trace at around 320°C. This interference thus generated substantial negative ΣANs
15 signal when we subtract the 180°C channel from 380°C channel. Indeed, significant portions
16 of uncorrected night time ΣANs signals throughout the campaign yielded negative values
17 including negative spikes correlated with positive NO₂ spikes from nearby road traffic
18 emissions. This effect was most prominent when high NO₂ concentration existed so that the
19 excess ΣANs signal was relatively small on the 380°C channel. Considering that under the
20 same O₃ concentration the fraction of NO₂ converted due to O atom chemistry was a constant,
21 larger overall NO₂ concentration corresponded to a larger overall NO₂ reduction which could
22 easily overwhelm the original ΣANs signal to introduce negative values when high
23 temperature channel was subtracted from lower temperature ones. For example, we have
24 performed high temperature box model simulations on O₃ pyrolysis reactions inside the TD
25 oven with a residence time of 0.17 second. At an O₃ concentration of 30 ppb the amount of
26 NO₂ loss through 380°C was around 6%. This indicates that if the ΣANs fraction within a
27 sample is less than 6% of the total concentration from NO₂, ΣPNs and ΣANs combined, a
28 negative value will result. The O atom chemistry outlined in Reactions (R4)–(R7) was further
29 complicated by the presence of organics, especially when initial NO₂ concentration was small
30 as signal loss in lab experiments was always more than can be explained in the absence of
31 organics. Since we were uncertain of the effect of possible chain reactions involving organic
32 radicals initiated by O atom, an empirical equation derived directly from in-lab observations
33 under NO_x and O₃ concentrations relevant to UBWOS condition was currently used for such

1 correction. Eq. (A1) shows the relation of fractional signal lost (r) as a function of the
2 observed total signal S_{380} of the 380°C channel ($\text{NO}_2 + \Sigma\text{PNs} + \Sigma\text{ANs}$) and O_3 concentration
3 with all parameters obtained through fitting of experimental data. The corrected signal (S'_{380})
4 was thus obtained with Eq. (A2).

$$5 \quad r = (0.0694 \times \ln(S_{380}) - 0.308) \times (0.0115 \times [\text{O}_3] + 0.557) \quad (\text{A1})$$

$$6 \quad S'_{380} = \frac{S_{380}}{1+r} \quad (\text{A2})$$

7

8 **Appendix B: VOC α calculation considering multiple generation RO_2 formation**

9 Explicit examples for calculating α are given in the following sections for OH-initiated
10 oxidation of ethane and propane in the presence of NO. Further generalizations to other
11 organics are also described.

12

13 **B1 α For Ethane**

14 Estimating α for ethane is relatively straightforward. Daytime oxidation of ethane starts with
15 an initial hydrogen extraction by OH radical followed by O_2 addition to the alkyl radical
16 formed. Only a single isomer of alkyl peroxy radical is involved and no significant
17 decomposition channel exists for the ethyl alkoxy radical formed from NO reaction that does
18 not yield organic nitrate, as shown in Figure B1. We simply state here and will demonstrate in
19 later section that the dominant fate of RO_2 radicals in the basin were reaction with NO
20 because $\text{RO}_2\text{-RO}_2$ and $\text{RO}_2\text{-HO}_2$ reactions are minor during the day. The number in bracket is
21 specific branching ratio of the processes represented. Branching ratios yielding organic
22 nitrates are colored in blue. The overall nitrate branching ratio in this simple case is the same
23 as the specific branching ratio of the ethylperoxy radical at 0.019.

24

25 **B2 α For Propane**

26 To calculate the overall nitrate yield for propane, the dominant product channels should be
27 traced, as illustrated in Figure B2. Two isomers are formed through hydrogen extractions
28 from either the primary or secondary carbon, giving n-propylperoxy and iso-propylperoxy
29 radical in a relative yield of 24% and 76%, respectively. The overall nitrate branching ratio

1 can then be calculated if the specific α for each peroxy isomer is known. Starting from n-
2 propylperoxy radical, the direct reaction with NO gives n-propyl nitrate with a relative yield
3 of 2.1% calculated according to the Carter and Atkinson's method at 273K and 842 mBar,
4 representative of campaign condition. The remaining portion of the channel proceeding
5 through alkoxy radical reactions has a further branching of decomposition reaction (rather
6 than reacting with O₂) to form a formaldehyde and an ethyl radical which promptly reacts
7 with O₂ to give ethylperoxy radical. The relative yield of decomposition versus O₂ reaction
8 can be calculated from the respective reaction rates reported in the literature. We used a
9 decomposition rate of 846 1/s (Curran, 2006) and the product of O₂ reaction rate with O₂
10 concentration giving a first-order rate constant of $4 \times 10^4 \text{ s}^{-1}$ for the O₂ channel. Branching
11 ratios are hence 2% and 98% for decomposition and O₂ reaction. The ethylperoxy radical
12 from the decomposition channel can then react further with NO to give organic nitrates with a
13 yield of 0.019, calculated in the previous section. Summing up both yields scaled by the
14 individual channel strength, we have the specific nitrate yield of n-propylperoxy radical as:
15 $(0.019 \times 0.02 \times 0.979 + 0.021) = 0.021$. Note the correction from the additional ethylperoxy
16 radical nitrate yield is almost negligible, due to the decomposition channel strength of only
17 2%. However, for larger molecules, typically starting from n-butane, isomerization reactions
18 can contribute substantially and higher-generation nitrate yield corrections are generally non-
19 negligible. For iso-propylperoxy radical the specific nitrate yield was calculated using the
20 same principle, only that after decomposition reaction a methylperoxy radical is formed.
21 Since methylperoxy radical has little yield for methyl nitrate formation, the total specific
22 nitrate yield for iso-propylperoxy radical is just the direct yield of 5.2%. The overall α for
23 propane-OH reaction is hence the ensemble average of the specific nitrate yield of all peroxy
24 isomers, namely: $(0.24 \times 0.021 + 0.76 \times 0.052) = 0.045$.

25

26 **B3 α For Higher Alkanes And Other Organics**

27 Using the method detailed above for propane, we carried out an extended estimation for
28 alkanes up to undecane which is the largest alkane reported from GC-MS data. The results are
29 summarized in Table 2. It is noted here that certain simplifications were necessary for this
30 calculation. For example, in estimating α for more complex RO₂ radicals from higher-
31 generation oxidation products we ignored the possible contribution of other oxygen-
32 containing functional groups toward the estimated yield given by the Carter and Atkinson

1 parameterization so that only carbon number was considered. Further, rate constants used to
2 estimate the relative branching ratios of alkoxy radical reactions were limited to available
3 literature values, generally around 298K. As carbon chain length becomes longer,
4 experimental data regarding O₂ reaction, isomerization and decomposition rates become
5 scarce and the data available for the most similar structure are used.

6

7 **Appendix C: Differences in definition of γ used in this work**

8 The γ value, used to denote the amount of O₃ molecule generated from OH-initiated oxidation
9 of an organic molecule in this work, is different from the definition of previous works that
10 focus on only single generation RO₂ chemistry in 2 respects, described as following. First, γ
11 has commonly been given a value of 2 for two O₃ molecules being generated per OH-initiated
12 oxidation of VOCs, from the formation of HO₂ and NO₂ each. This is a good approximation
13 for small alkanes of which isomerization is not important, but can be erroneous otherwise. For
14 example, in the absence of organic nitrate formation channel, we estimate γ for n-hexane to be
15 3.2 due to the efficient isomerization reaction of hydrogen abstraction by the 2-alkoxy or 3-
16 alkoxy radical produced, generating a new alkyl radical and an alcohol group. The presence of
17 large alkanes, up to undecane, necessitates a more careful treatment. Second, γ has been used
18 to calculate the ratio of O₃ production rate over Σ ANs production rate, formulated as $\gamma(1-\alpha)/\alpha$.
19 The factor (1- α) in the numerator implies that γ was estimated under the assumption of zero
20 nitrate formation. (1- α) therefore accounted for the fraction of reaction that actually proceeded
21 to form O₃. This is only exact if VOC + OH reaction only forms a single generation of RO₂
22 molecule, once again a valid assumption for small VOC only. For larger alkanes there exist a
23 non-negligible fraction of higher generation RO₂ reactions from isomerization reactions and
24 we must account for the effective number of NO₂ and HO₂ formed in a cumulative manner
25 over extended generations. This means γ and α are related by the structure of the molecule
26 under consideration. Our listed γ values in table 2 is then the better average number of O₃
27 generated per OH-initiated oxidation with alkyl nitrate formation considered, or in the same
28 spirit, the “ $\gamma(1-\alpha)$ ” value considered over multi-generation reactions. In Table 2, we observe
29 an increasing trend of γ going from methane to around hexane as larger alkanes are more
30 susceptible to isomerization and further radical reactions, converting more NO to NO₂. This
31 trend does not continue, however, with further increase of alkane size because of the

1 competing effect of increasing organic nitrate yield, eventually reduces the amount of alkoxy
2 radical formed.

3

4 **Acknowledgements**

5 The authors acknowledge the NOAA office of global programs: NA13OAR4310067 and NSF
6 AGS-1120076 for their support of this research. The authors also acknowledge Jim Roberts
7 for his hospitality and support in PAN, HONO and ClNO₂ data, and Brian Lerner for VOC
8 data.

9

1 **References**

- 2 Atkinson, R., Carter, W. P. L., and Winer, A. M.: Effects of temperature and pressure on alkyl
3 nitrate yields in the NO_x photooxidations of normal-pentane and normal-heptane, *J. Phys.*
4 *Chem.*, 87, 2012-2018, 10.1021/j100234a034, 1983.
- 5 Atkinson, R., and Aschmann, S. M.: Rate constants for the gas-phase reactions of the OH
6 radical with a series of aromatic-hydrocarbons at 296 +/- 2K, *Int. J. Chem. Kinet.*, 21, 355-
7 365, 10.1002/kin.550210506, 1989.
- 8 Atkinson, R.: *Gas-Phase Tropospheric Chemistry of Organic-Compounds*, *J. Phys. Chem.*
9 *Ref. Data*, ISBN: 156396340X, 1994.
- 10 Atkinson, R., Baulch, D. L., Cox, R. A., Crowley, J. N., Hampson, R. F., Hynes, R. G.,
11 Jenkin, M. E., Rossi, M. J., and Troe, J.: Evaluated kinetic and photochemical data for
12 atmospheric chemistry: Volume I - gas phase reactions of O(x), HO(x), NO(x) and SO(x)
13 species, *Atmos. Chem. Phys.*, 4, 1461-1738, 2004.
- 14 Atkinson, R., Baulch, D. L., Cox, R. A., Crowley, J. N., Hampson, R. F., Hynes, R. G.,
15 Jenkin, M. E., Rossi, M. J., and Troe, J.: Evaluated kinetic and photochemical data for
16 atmospheric chemistry: Volume II - gas phase reactions of organic species, *Atmos. Chem.*
17 *Phys.*, 6, 3625-4055, 2006.
- 18 Carter, W. P. L., and Atkinson, R.: Alkyl Nitrate Formation From the Atmospheric
19 Photooxidation of Alkanes - a Revised Estimation Method, *Journal of Atmospheric*
20 *Chemistry*, 8, 165-173, 10.1007/bf00053721, 1989.
- 21 Curran, H. J.: Rate constant estimation for C-1 to C-4 alkyl and alkoxy radical
22 decomposition, *Int. J. Chem. Kinet.*, 38, 250-275, 10.1002/kin.20153, 2006.
- 23 Day, D. A., Wooldridge, P. J., Dillon, M. B., Thornton, J. A., and Cohen, R. C.: A thermal
24 dissociation laser-induced fluorescence instrument for in situ detection of NO(2), peroxy
25 nitrates, alkyl nitrates, and HNO(3), *J. Geophys. Res.-Atmos.*, 107, ACH 4-1-ACH 4-14,
26 10.1029/2001jd000779, 2002.
- 27 Droege, A. T., and Tully, F. P.: Hydrogen-atom abstraction from alkanes by OH .3. Propane,
28 *J. Phys. Chem.*, 90, 1949-1954, 10.1021/j100400a042, 1986.
- 29 Edwards, P. M., Young, C. J., Aikin, K., deGouw, J., Dube, W. P., Geiger, F., Gilman, J.,
30 Helmig, D., Holloway, J. S., Kercher, J., Lerner, B., Martin, R., McLaren, R., Parrish, D. D.,

1 Peischl, J., Roberts, J. M., Ryerson, T. B., Thornton, J., Warneke, C., Williams, E. J., and
2 Brown, S. S.: Ozone photochemistry in an oil and natural gas extraction region during winter:
3 simulations of a snow-free season in the Uintah Basin, Utah, *Atmos. Chem. Phys.*, 13, 8955-
4 8971, 10.5194/acp-13-8955-2013, 2013.

5 Farmer, D. K., Perring, A. E., Wooldridge, P. J., Blake, D. R., Baker, A., Meinardi, S., Huey,
6 L. G., Tanner, D., Vargas, O., and Cohen, R. C.: Impact of organic nitrates on urban ozone
7 production, *Atmos. Chem. Phys.*, 11, 4085-4094, 10.5194/acp-11-4085-2011, 2011.

8 Gery, M. W., Fox, D. L., Jeffries, H. E., Stockburger, L., and Weathers, W. S.: A continuous
9 stirred tank reactor investigation of the gas-phase reaction of hydroxyl radicals and toluene,
10 *Int. J. Chem. Kinet.*, 17, 931-955, 10.1002/kin.550170903, 1985.

11 Goldan, P. D., Kuster, W. C., Williams, E., Murphy, P. C., Fehsenfeld, F. C., and Meagher, J.:
12 Nonmethane hydrocarbon and oxy hydrocarbon measurements during the 2002 New England
13 Air Quality Study, *J. Geophys. Res.-Atmos.*, 109, D21309, 10.1029/2003jd004455, 2004.

14 Grund, C. J., Banta, R. M., George, J. L., Howell, J. N., Post, M. J., Richter, R. A., and
15 Weickmann, A. M.: High-resolution Doppler lidar for boundary layer and cloud research, *J.*
16 *Atmos. Ocean. Tech.*, 18, 376-393, 10.1175/1520-0426(2001)018<0376:hrdlfb>2.0.co;2,
17 2001.

18 Kliner, D. A. V., Daube, B. C., Burley, J. D., and Wofsy, S. C.: Laboratory investigation of
19 the catalytic reduction technique for measurement of atmospheric NO_y, *J. Geophys. Res.-*
20 *Atmos.*, 102, 10759-10776, 10.1029/96jd03816, 1997.

21 Luke, W. T., Dickerson, R. R., and Nunnermacker, L. J.: Direct measurements of the
22 photolysis rate coefficients and Henry law constants of several alkyl nitrates, *J. Geophys.*
23 *Res.-Atmos.*, 94, 14905-14921, 10.1029/JD094iD12p14905, 1989.

24 Neuman, J. A., Aikin, K. C., Atlas, E. L., Blake, D. R., Holloway, J. S., Meinardi, S., Nowak,
25 J. B., Parrish, D. D., Peischl, J., Perring, A. E., Pollack, I. B., Roberts, J. M., Ryerson, T. B.,
26 and Trainer, M.: Ozone and alkyl nitrate formation from the Deepwater Horizon oil spill
27 atmospheric emissions, *J. Geophys. Res.-Atmos.*, 117, D09305, 10.1029/2011jd017150,
28 2012.

29 Perring, A. E., Bertram, T. H., Wooldridge, P. J., Fried, A., Heikes, B. G., Dibb, J., Crouse,
30 J. D., Wennberg, P. O., Blake, N. J., Blake, D. R., Brune, W. H., Singh, H. B., and Cohen, R.

1 C.: Airborne Observations of Total RONO₂: New Constraints on the Yield and Lifetime of
2 Isoprene Nitrates, *Atmos. Chem. Phys.*, 9, 1451-1463, 2009.

3 Perring, A. E., Bertram, T. H., Farmer, D. K., Wooldridge, P. J., Dibb, J., Blake, N. J., Blake,
4 D. R., Singh, H. B., Fuelberg, H., Diskin, G., Sachse, G., and Cohen, R. C.: The production
5 and persistence of Sigma RONO₂ in the Mexico City plume, *Atmos. Chem. Phys.*, 10, 7215-
6 7229, 10.5194/acp-10-7215-2010, 2010.

7 Perring, A. E., Pusede, S. E., and Cohen, R. C.: An observational perspective on the
8 atmospheric impacts of alkyl and multifunctional nitrates on ozone and secondary organic
9 aerosol, *Chem. Rev.*, 113, 5848-5870, 10.1021/cr300520x, 2013.

10 Roberts, J. M., Osthoff, H. D., Brown, S. S., Ravishankara, A. R., Coffman, D., Quinn, P.,
11 and Bates, T.: Laboratory studies of products of N₂O₅ uptake on Cl⁻ containing substrates,
12 *Geophys. Res. Lett.*, 36, L20808, 10.1029/2009gl040448, 2009.

13 Rosen, R. S., Wood, E. C., Wooldridge, P. J., Thornton, J. A., Day, D. A., Kuster, W.,
14 Williams, E. J., Jobson, B. T., and Cohen, R. C.: Observations of total alkyl nitrates during
15 Texas Air Quality Study 2000: implications for O₃ and alkyl nitrate photochemistry, *J.*
16 *Geophys. Res.*, 109, 15 pp.-15 pp., 10.1029/2003jd004227, 2004.

17 Schnell, R. C., Oltmans, S. J., Neely, R. R., Endres, M. S., Molenaar, J. V., and White, A. B.:
18 Rapid photochemical production of ozone at high concentrations in a rural site during winter,
19 *Nat. Geosci.*, 2, 120-122, 10.1038/ngeo415, 2009.

20 Thaler, R. D., Mielke, L. H., and Osthoff, H. D.: Quantification of nitryl chloride at part per
21 trillion mixing ratios by thermal dissociation cavity ring-down spectroscopy, *Anal. Chem.*, 83,
22 2761-2766, 10.1021/ac200055z, 2011.

23 Thornton, J. A., Wooldridge, P. J., and Cohen, R. C.: Atmospheric NO₂: In Situ Laser-
24 Induced Fluorescence Detection at Parts Per Trillion Mixing Ratios, *Anal. Chem.*, 72, 528-
25 539, 10.1021/ac9908905, 2000.

26 Wagner, N. L., Dube, W. P., Washenfelder, R. A., Young, C. J., Pollack, I. B., Ryerson, T. B.,
27 and Brown, S. S.: Diode laser-based cavity ring-down instrument for NO₃, N₂O₅, NO, NO₂
28 and O₃ from aircraft, *Atmos. Meas. Tech.*, 4, 1227-1240, 10.5194/amt-4-1227-2011, 2011.

1 Table 1. Median OH reactivity and associated formation rates at local noon.

Compound Class	OH Reactivity (s ⁻¹)	p(Σ ANs) ^r (ppt·hr ⁻¹)	p(O ₃) ^r (ppt·hr ⁻¹)
Alkane C ₁ -C ₁₁	5.02	172	1760
Alkene C ₂ -C ₃	0.15	0.71	44
Alkyne C ₂	0.013	0	2.4
Aromatic C ₆ -C ₉	0.58	0.90	120
Alcohol C ₁ -C ₂	0.31	0	48
Ketone C ₃ -C ₄	0.0084	~0	0.37
Aldehyde C ₁ -C ₄	0.44	0	130
CO	0.95	0	150
NO	0.61	0	0
NO ₂	0.82	0	0
Total	8.90	174	2250

* Median noon time [OH] = 1×10⁶ molecule cm⁻³

2

1 Table 2. Summary of specific organic nitrate and ozone yield calculated at 0°C

Compound Class	α	γ	Compound Class	α	γ
Alkane	0.22	2.25	Alkene	0.031	1.94
methane	~0	2	ethene	0.025	1.95
ethane	0.019	1.96	propene	0.05	1.9
propane	0.045	1.92	Alkyne	0	1.2
iso-butane	0.11	2.6	ethyne	~0	1.2
n-butane	0.114	2.17	Aromatic	0.01^a	1.3^b
iso-pentane	0.21	2.46	Alcohol	0	1
n-pentane	0.2	2.19	methanol	~0	1
2,2-dimethylpropane	0.25	3.1	ethanol	~0	1.05
n-hexane	0.42	2.62	Ketone	0.077	3.72
2,2-dimethylbutane	0.36	2.7	acetone	0.021	4
2-methylpentane	0.29	2.2	methylethylketone	0.11	3.56
3-methylpentane	0.33	2.34	Aldehyde	0	1.96
methyl-cyclopentane	0.29	2.9	formaldehyde	0	1
Cyclohexane	0.33	2	acetaldehyde	0	3
methyl-cyclohexane	0.58	2.4	propanal	0.019	3
ethyl-cyclohexane	0.5	2.25	butanal	0.045	2.91
dimethyl-cyclohexane	0.67	1.8	methacrolein	0.05	2.45
heptane	0.6	2.2			
octane	0.6	1.86			
nonane	0.62	1.52			
decane	0.74	1.43			
undecane	0.81	1.2			

^a Previously assumed value of 0.1 is due to contribution of nitrobenzene which we do not detect in Σ ANs channel.

^b Assumption based on toluene data.

2

3

1 Table 3. Expected maximum O_x (NO₂ + O₃) concentration under UBWOS condition

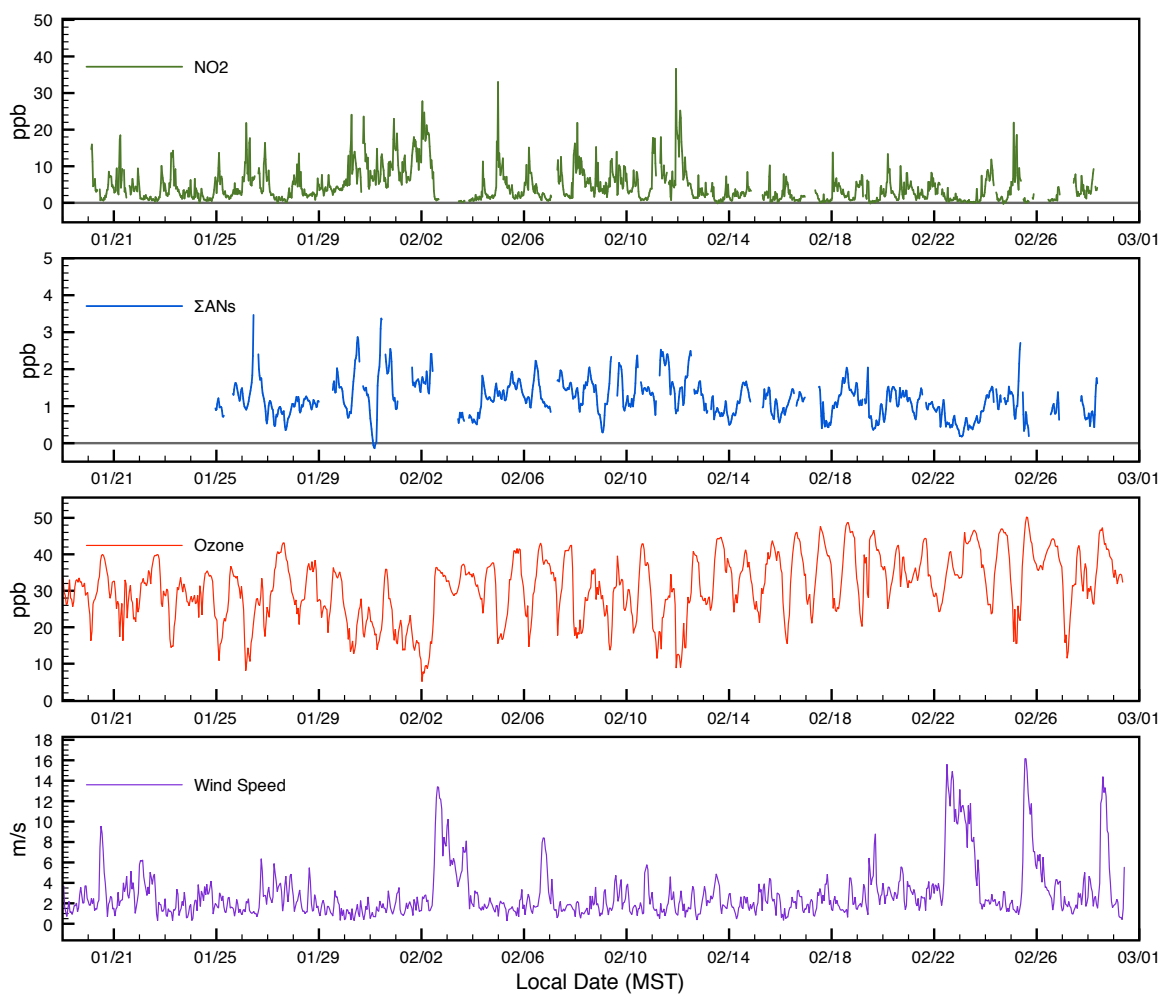
Condition ^b	UBWOS 2012 base condition	photolysis × 2 & mixing ÷ 2
α calculated at 273K ^a	57 ppb	140 ppb
α calculated at 300K ^a	64 ppb	165 ppb
difference	7±4 ppb ^c	25±15 ppb ^c

^a Carter and Atkinson, 1989.

^b Assuming background O₃ concentration of 30 ppb.

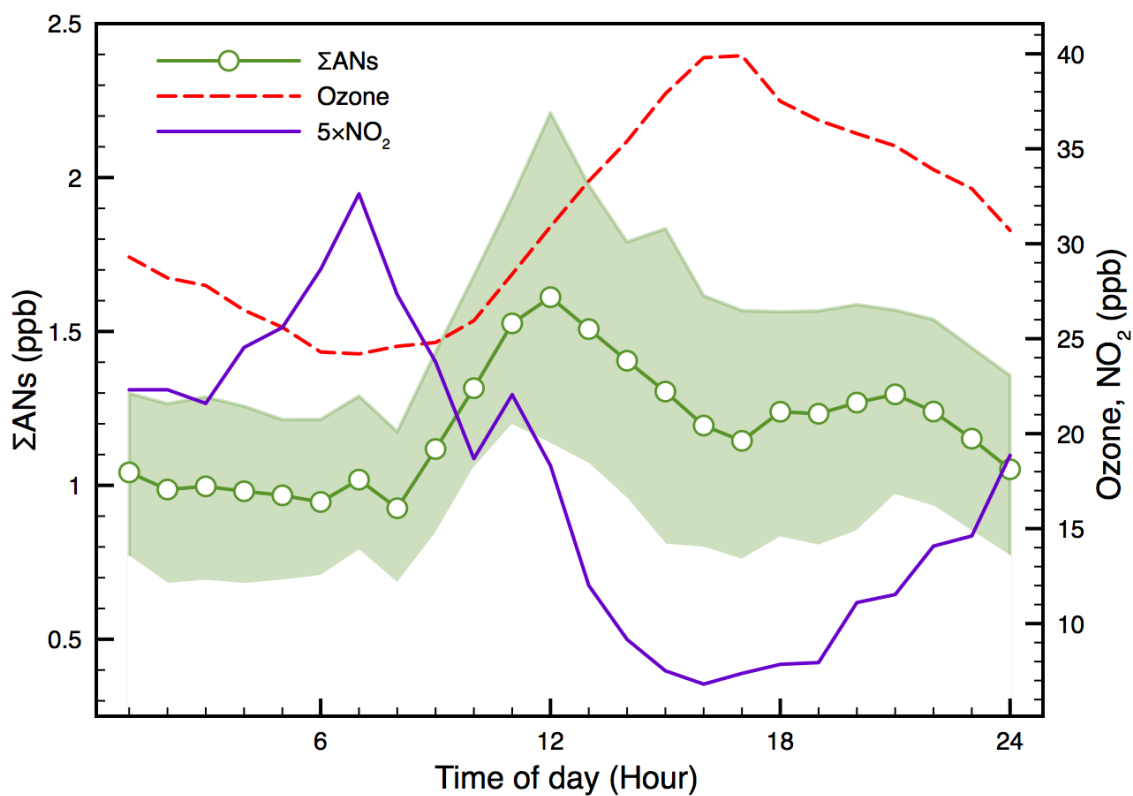
^c Uncertainty due to temperature dependence parameterization of alkyl nitrate yield.

2

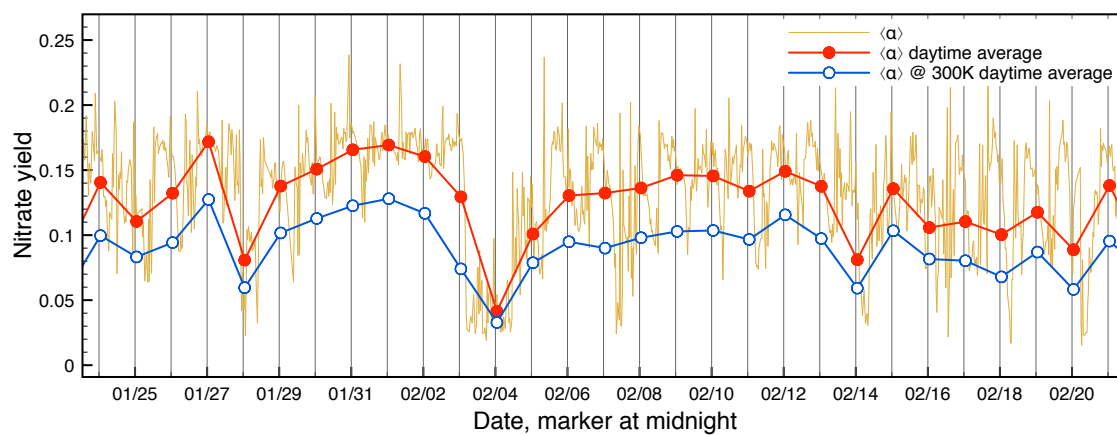


1
 2
 3 Figure 1. Hourly-averaged time series of NO₂, total alkyl nitrates (ΣANs), O₃ and windspeed
 4 measured during UBWOS 2012. The concentrations are measured at height of 16 meters from
 5 a 19-meter scaffolding tower on site. The windspeed is measured at the tower top. Ticks on
 6 the x-axis mark local midnight.

7

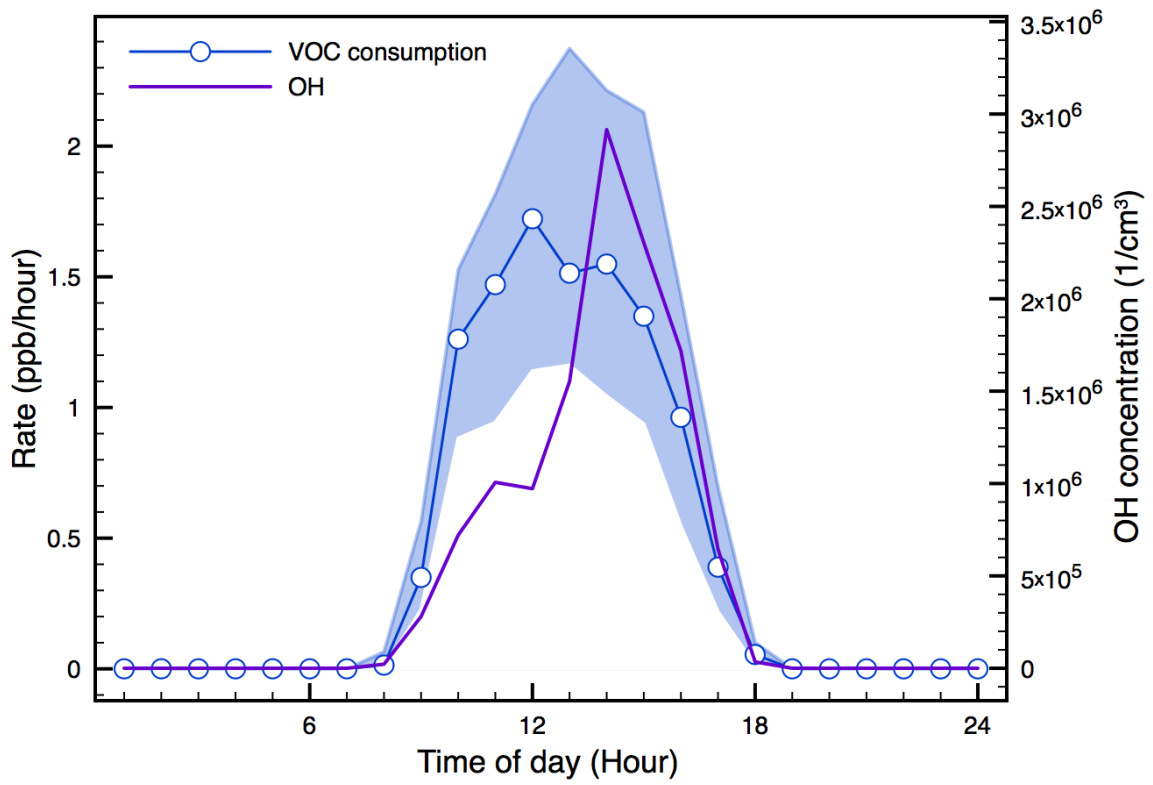


1
 2
 3 Figure 2. Diurnal variations of Σ ANs, ozone and NO_2 . Lines represent median values while
 4 the shaded area of Σ ANs represents the interquartile (25–75%) coverage. The Σ AN data have
 5 been corrected for O_3 interference and the ClNO_2 contribution has been subtracted (see text).
 6



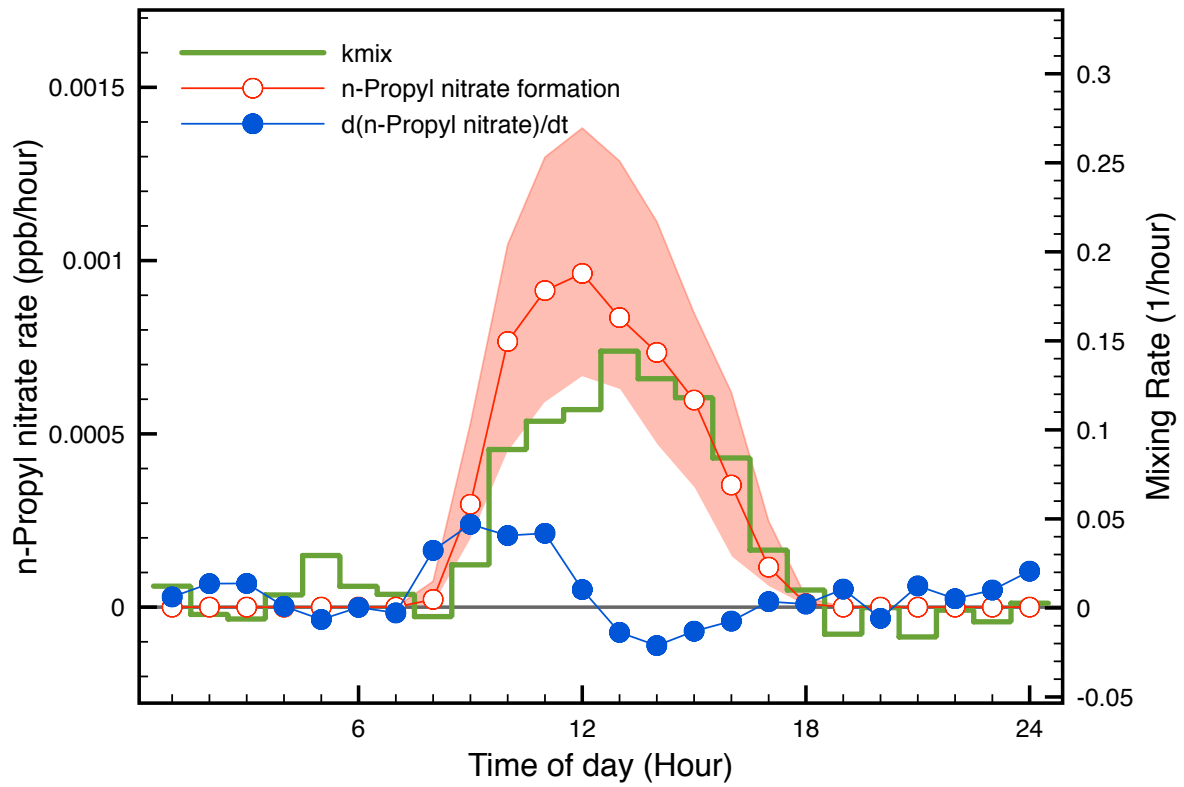
1
2
3
4
5
6
7

Figure 3. Ensemble-averaged nitrate formation yield ($\langle \alpha \rangle$) calculated based on the method in section 3.2.1. Red symbols represent daytime average of the hourly $\langle \alpha \rangle$ (in orange) estimated at 273K, representative of the campaign period conditions. The blue symbols are the daytime averaged $\langle \alpha \rangle$ estimated at 300K, routinely used in global models.



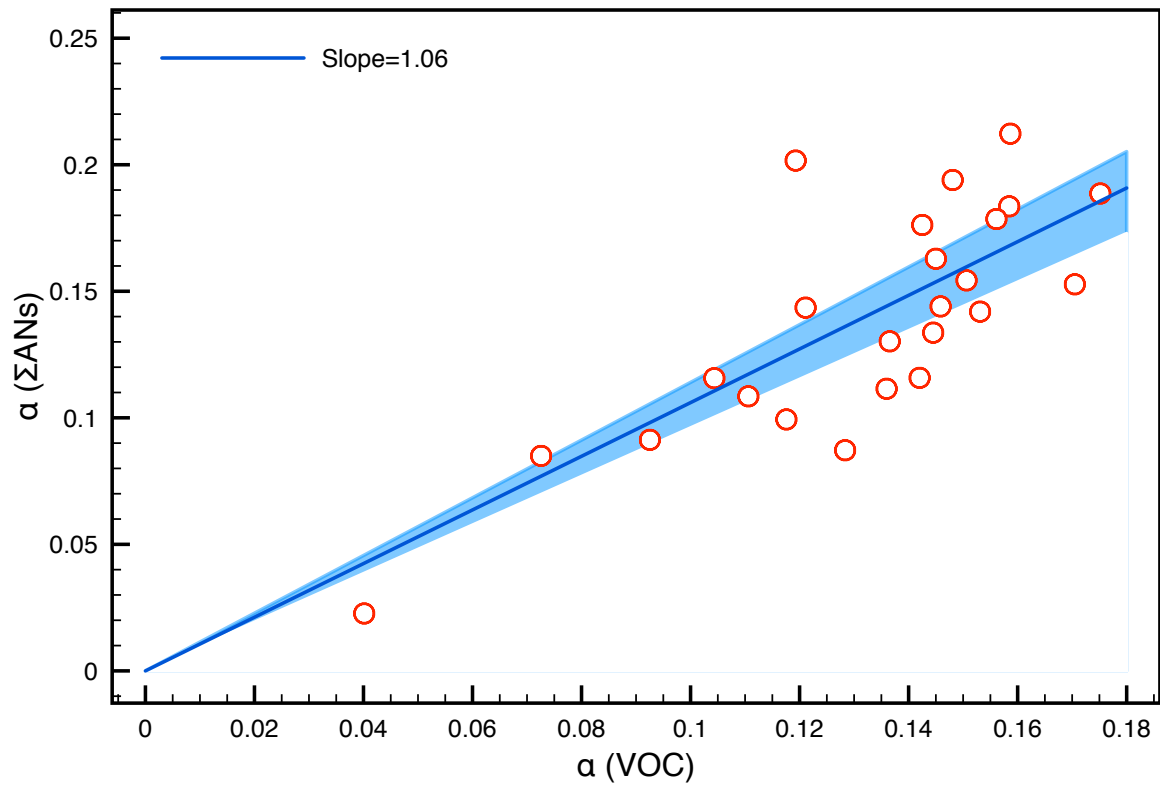
1
2
3
4
5
6
7

Figure 4. Calculated daytime median profiles of the VOC consumption rate and the OH concentration. The VOC consumption rate is controlled by the photolysis rate leading to OH and HO₂ radical formation, while OH concentration is regulated by the OH reactivity dominated by the NO_x and VOC concentrations.



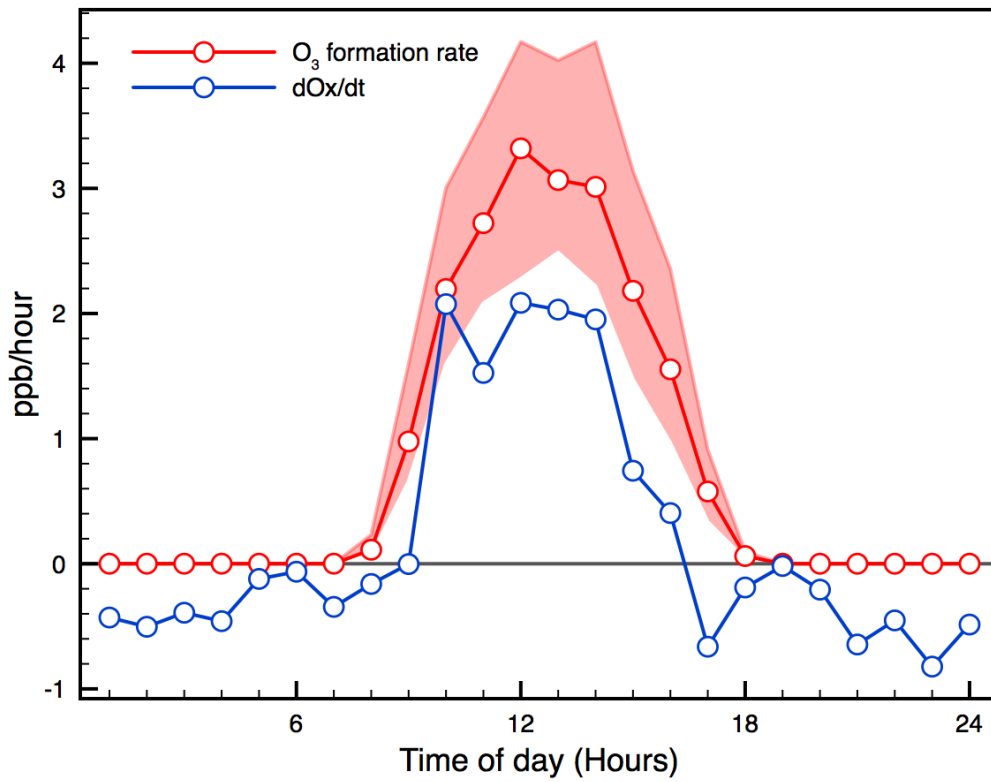
1
2
3
4
5
6
7

Figure 5. The production rate and concentration change of n-propyl nitrate calculated from field observations. The difference between the red and blue traces represent the mixing loss promoted by solar surface heating. The green trace is the calculated effective first order mixing rate, k_{mix} .



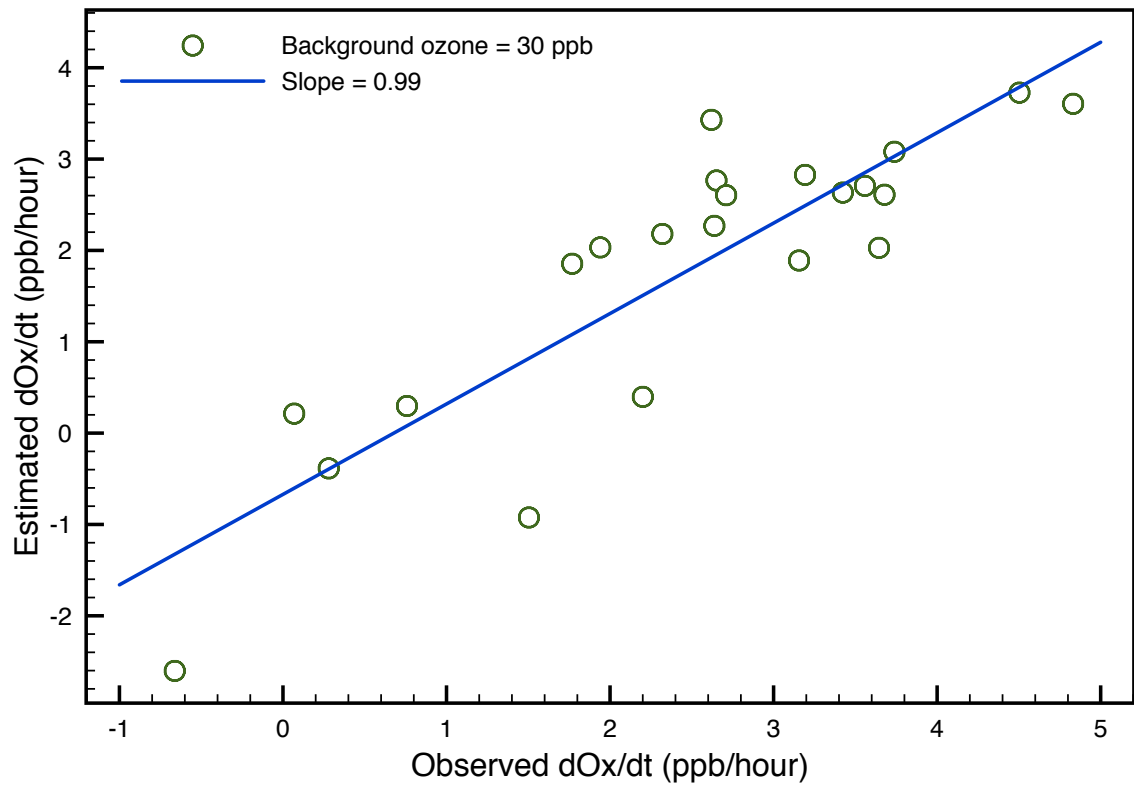
1
2
3
4
5
6
7

Figure 6. Correlation between daytime averaged α estimated using the VOC-ensemble method (VOC, section 3.2.1) and oxidation-production method (Σ ANs, section 3.2.2). The shaded area corresponds to the 95% confidence interval for the regression slope passing through origin. The 1:1 line is within this interval.



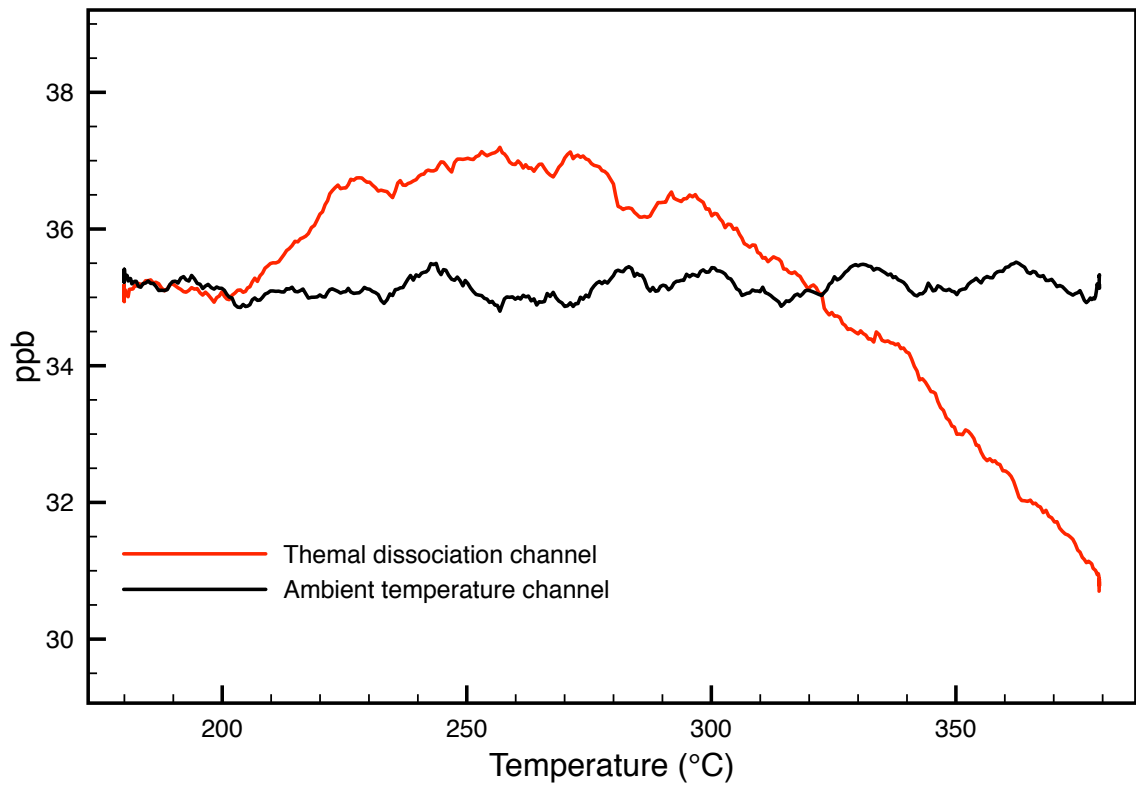
1
2
3
4
5
6
7

Figure 7. Calculated daytime O₃ formation rate and the rate of change of O_x (NO₂ + O₃) observed. The difference between traces can be attributed to mixing using the same mixing rate estimated from n-propyl nitrate. The existence of non-negligible background O₃ concentration (30 ppb) suppresses the net dilution.



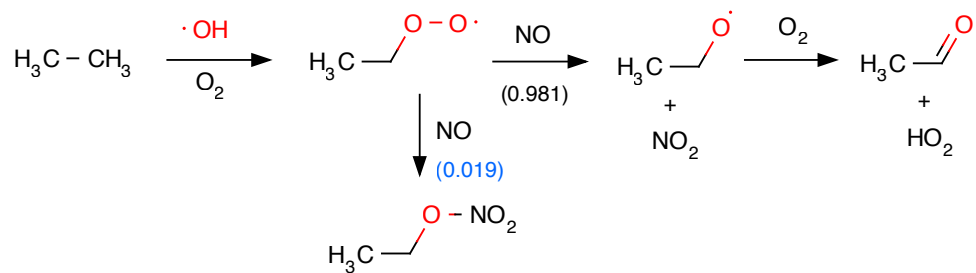
1
2
3
4
5
6

Figure 8. Correlation of the estimated daytime hourly O₃ production rate corrected for dilution loss to what was observed from O₃ and NO₂ data. A background O₃ concentration of 30 ppb was assumed.



1
2
3
4
5
6

Figure A1. Laser induced fluorescence signal from samples containing ~35 ppb NO₂ and 2 ppb 2-ethylhexyl nitrate passing through the unheated channel (ambient temperature, black trace) and thermal dissociation channel (red trace) in the presence of O₃.

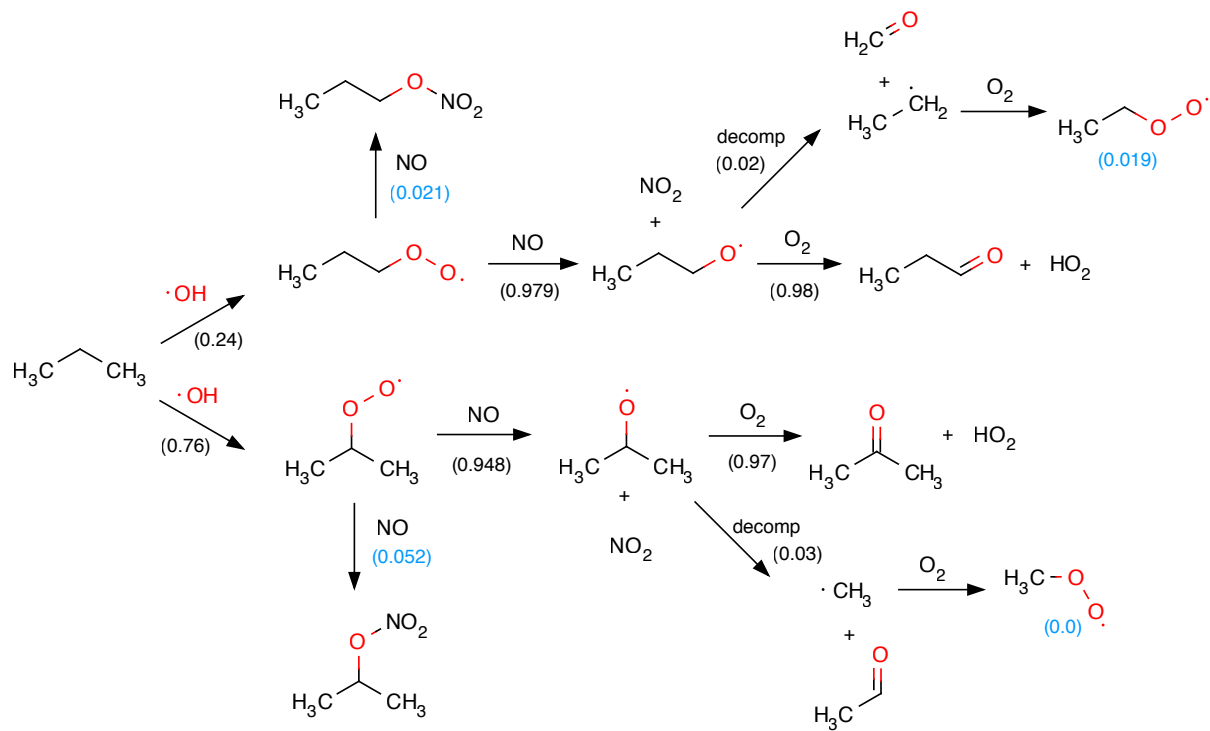


1

2

3 Figure B1. Ethane oxidation by OH radical in the presence of NO.

4



1

2

3 Figure B2. Propane oxidation by OH radical in the presence of NO.